# Photoresponsive Organic Cages – Computationally Driven Discovery of Azobenzene-Derived Organic Cages

Michael C. Brand,[a,b] Hamish G. Trowell,[c] James T. Pegg,[c] Jake L. Greenfield,[c,d] Magdalena Odaybat,[c] Marc A. Little,[a,e] Peter R. Haycock,[c] Nicola Rankin,[a,b] Matthew J. Fuchter,[c] Kim E. Jelfs,[c] Andrew I. Cooper[a,b] and Rebecca L. Greenaway[a,c]*

[a]Department of Chemistry and Materials Innovation Factory, University of Liverpool, 51 Oxford Street, Liverpool, L7 3NY, U.K.

[b]Leverhulme Research Centre for Functional Materials Design, Materials Innovation Factory and Department of Chemistry, University of Liverpool, L7 3NY, U.K.

[c]Department of Chemistry, Imperial College London, White City Campus, Wood Lane, London, W12 0BZ, U.K.

[d]Institut für Organische Chemie, Universität Würzburg, 97074 Würzburg, Germany

[e]Institute of Chemical Sciences, Heriot-Watt University, Edinburgh, U.K.

Email: r.greenaway@imperial.ac.uk

**The incorporation of photoresponsive groups into porous materials is attractive as it offers potential advantages in controlling the pore size and selectivity to guest molecules. A combination of computational modelling and experiment resulted in the synthesis of two azobenzene-derived organic cages based on building blocks identified in a computational screen. Both cages incorporate three azobenzene moieties, and are therefore capable of three-fold isomerization, using either ditopic or tetratopic aldehydes containing diazene functionality. The ditopic aldehyde forms a $Tri^2Di^3$ cage via a 6-fold imine condensation and the tritopic aldehyde forms a $Tet^3Di^6$ cage via a 12-fold imine condensation. The relative energies and corresponding intrinsic cavities of each isomeric state were computed, and the photoswitching behaviour of both cages was studied by UV–Vis and $^1H$ NMR spectroscopy, including a detailed kinetic analysis of the thermal isomerization for each of the *EEZ*, *EZZ* and *ZZZ* metastable isomers of the $Tet^3Di^6$ cage. Both cages underwent photoisomerization, where a photostationary state of up to 77% of the cis-isomer and overall thermal half-life of 110 hours was identified for the $Tet^3Di^6$ species. Overall, this work demonstrates the potential of computational modelling to inform the design of photoresponsive materials and highlights the contrasting effects on the photoswitching properties of the azobenzene moieties on incorporation into the different cage species.**

## Introduction

Porous materials have applications in processes such as petrochemical refining[1] and the separation of gases[2] and solvents.[3] In recent years, multicomponent self-assembled materials have emerged as an important class of porous materials. This includes porous coordination polymers and metal-organic frameworks (MOFs) formed through coordination chemistry, and covalent-organic frameworks (COFs) and porous organic cages (POCs) typically formed using dynamic covalent chemistries, such as imine condensations.[4] POCs are 3-dimensional discrete organic molecules that contain a permanent internal cavity that is accessible through multiple windows.[5] POCs can be formed into molecular solids, but lack the extended coordination or covalent bonding networks found in MOFs and COFs. However, POCs can pack together in the solid-state to form interconnected pore networks,[6] and they have shown potential in the molecular separation of gases,[7] hydrogen isotopes,[8] and organic compounds.[9] Additionally, POCs have been used as molecular sensors,[10] and due to their discrete nature and solution processability, they have been incorporated into a new generation of porous materials known as porous liquids; that is, liquids that contain permanent intrinsic porosity.[11]

The integration of stimuli-responsive moieties into porous materials such as MOFs and COFs can result in materials that are capable of a structural switch between two or more isomeric states.[12] To induce a response, the energy input can be by photochemical irradiation,[13] mechanical stress,[14] or electrostatic stimulation.[15] There are several benefits to incorporating stimuli-responsive functional groups in a porous material, including the ability to change the internal pore size allowing for on/off selectivity of gases, or to spontaneously release gas from within the porous material,[16] or to block the pore windows enabling gas storage through a trapping technique.[17] Several compounds undergo isomerization upon irradiation with UV–visible light (photoisomerization), including stilbenes,[18] azobenzenes,[19] diarylethenes,[20] spiropyrans,[21] and imines.[22] Here, azobenzenes were selected for their reversible *E*–*Z* isomerization (Fig. 1a) which can have a dramatic effect on the molecular geometry of the species they are incorporated into, compared to the more subtle bond rearrangements found in diarylethenes.[13b]

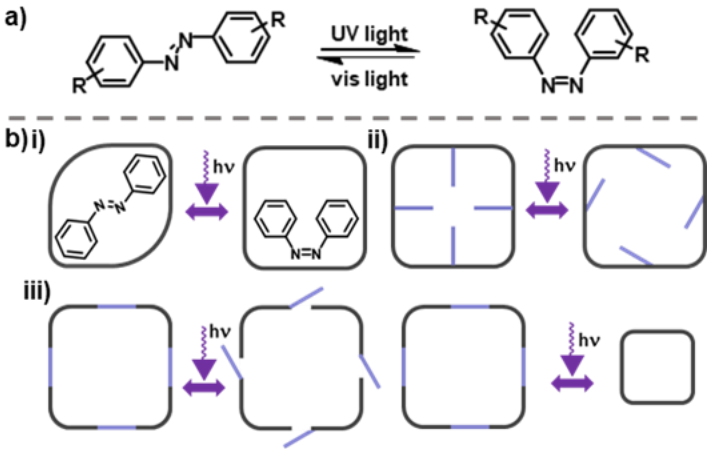


**Figure 1.** (a) Isomerization of azobenzene: the *E*→*Z* isomerization can be controlled through irradiation of the π–π* transition at a wavelength of ~320 nm, *Z*→*E* isomerization can be controlled by irradiation of the n–π* transition at a wavelength ~450 nm, or through heating; (b) Representation of the different methods to integrate a photoresponsive moiety (shown in light purple) into a porous material: (i) loading with a photoactive guest; (ii) decorating with photoresponsive groups; (iii) incorporation of photoresponsive groups into the scaffold itself to either introduce a gating mechanism or induce a change in size and/or shape.

Azobenzenes' resistance to photodegradation makes them suitable for multiple uptake/release photoswitching cycles in porous materials compared to stilbenes[23] and spiropyrans.[24] There are several methods by which these photoresponsive moieties can be integrated into a porous material (Fig. 1b).[25] The first method includes addition of a photoresponsive guest – that is, a porous material is loaded with a photoactive guest (Fig. 1b(i)) and upon irradiation, a change is imposed on the host material.[26] Another method is the incorporation of photoresponsive auxiliaries (Fig. 1b(ii)). This second method typically has minimal effect in relation to a structural change, but rather, the pore can be filled, or the windows can be blocked or opened, through an *E*–*Z* isomerization.[27] A third method of integrating a photoresponsive group is to incorporate it directly into the molecular structure itself (Fig. 1b(iii)); for example, by the addition of photoresponsive linkers into a MOF.[28]

While the incorporation of photoswitchable moieties into coordination cages[29] and macrocycles[30] has been reported, the formation of stimuli-responsive POCs remains underexplored. Previous literature has focused on POCs formed exclusively from ditopic azobenzene precursors, linked either *via* imine or amine functionalities with examples demonstrating improved photostationary states upon POC formation,[31] differential reactivity towards imine exchange reactions upon switching,[32] and *p*-xylene separation through a crystal-to-crystal phase transition.[33] Oshchepkov *et al.* studied the ability of the same amine-linked cage for anion coordination and recognition by a larger cucurbit[8]uril host.[34] It can be envisaged that the introduction of a photoresponsive moiety into a POC could result in a dynamic reversible geometry change, leading to a controllable pore size and shape, which in turn might enable host–guest selectivity or the controlled uptake and release of different molecular guests in the cage.

Here we explore the incorporation of photoresponsive diazene precursors as one of the components of a covalent organic cage. Organic cages incorporating azobenzene functionality were first designed based on synthetically accessible precursors and investigated using computational methods, prior to investigation of synthetically viable cage structures in an experimental screen. Two azobenzene-covalent cages (ACC) were discovered; a novel **Tet$^3$Di$^6$** tubular cage (**ACC-1**) consisting of three tetratopic (Tet$^3$) aldehydes and six ditopic (Di$^6$) amines, and a **Tri$^2$Di$^3$** capsule (**ACC-2**) consisting of two tritopic (Tri$^2$) amines and three ditopic (Di$^3$) aldehydes, and their photoswitching behaviour investigated through a series of UV–Vis and $^1$H NMR spectroscopic studies. Each cage is capable of three-fold isomerization, using either ditopic or tetratopic aldehydes containing diazene functionality. The photoswitching behaviour of the two azobenzene moieties on incorporation into the cage structures was also investigated by comparing them to single azobenzene-imine subunits. Finally, with the **Tet$^3$Di$^6$** cage exhibiting superior photoswitching properties compared to the **Tri$^2$Di$^3$** cage, a detailed kinetic analysis of the thermal isomerization for each of its *EEZ*, *EZZ* and *ZZZ* metastable isomers was conducted.

**Results and Discussion**

Initially a computational screen was carried out with the aim of predicting *a priori* viable POCs that incorporate an azobenzene switch. Two azobenzene precursors were identified from the screen based on existing precursor scaffolds previously used in POC syntheses,[35] and their synthetic viability assessed based on known routes to azobenzenes, where the azobenzene was incorporated into the scaffold rather than as a pendant group. This resulted in ditopic and tetratopic aldehydes that were assembled computationally in both their *E*- and *Z*-conformations with seven ditopic and three tritopic amines into a range of candidate organic cages. This included three cages in each of the **Tri$^2$Di$^3$** and

**Tri$^4$Di$^6$** topologies for the ditopic aldehydes with tritopic amines, and seven cages in each of the **Tet$^2$Di$^4$** and **Tet$^3$Di$^6$** topologies for the tetratopic aldehydes with ditopic amines, where the superscripts signify the number of each of the precursors incorporated into the cage (Fig. 2).[36] For the tetratopic aldehyde systems, there are multiple connection possibilities, depending upon the relative arrangement of the tetratopic aldehyde. This means there are 2 positional isomers to consider for each **Tet$^2$Di$^4$** topology and 4 for each **Tet$^3$Di$^6$** topology. Thus, a total of 48 possible cages were modelled.

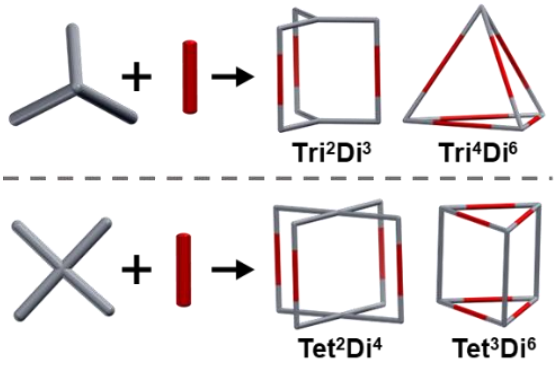


**Figure 2.** A combination of ditopic (Di), tritopic (Tri), and tetratopic (Tet) precursors and their possible assembled topological outcomes. The building block with the highest level of functionality is shown in grey in each case, the other in red.

After structural model assembly using our supramolecular toolkit (*stk*) software package,[37] the OPLS3e forcefield was used to geometry optimise each cage,[38] and a basic conformer search was carried out using gas-phase molecular dynamics (MD) simulations where 50 conformations were sampled over 200 ps. During this process, the torsion angles across the diazene moiety were constrained to prevent conversion between the *E*- and *Z*-isomers. The lowest-energy candidate cages were screened for shape-persistence and symmetry using *pyWindow*, open-source code for the determination of cavity size, the number of windows and diameter of windows for porous molecules.[39] The resulting cages were then inspected to identify promising candidates on the basis of being shape-persistent (having an internal cavity that can fit a sphere of diameter greater than 1 Å) and being largely symmetric (*i.e.*, all window diameters within 10% of each other). As a further filter, we visually inspected the structures to prioritize candidate molecules that were not overly strained; for example, by containing out-of-plane imine bonds. Cages where both the fully *trans* (*EEE*) and fully *cis* (*ZZZ*) forms satisfied the above criteria were hypothesised to be potentially photoisomerizable, not considering at this point energy barriers to interconversion. In general, the tetratopic diazene aldehyde was found to be more likely to form a photoisomerizable cage than the ditopic diazene aldehyde. This was also promising because it suggested the potential for a larger structural photoresponse, since the **Tet$^3$Di$^6$** topology results in larger molecular cages with more photoisomerizable linkers. Based on this computational screening, both the ditopic and tetratopic aldehyde were investigated experimentally.

A preliminary synthetic investigation was carried out into the cage formation between the tetratopic diazene aldehyde (for synthetic routes to precursors, see SI Section 2) in combination with (1*R*,2*R*)-cyclohexyldiamine (CHDA), using conditions similar to those previously reported for analogous tubular covalent cages (**TCC1-3**).[35a] In this initial screen, both solvent and concentration were varied, using conditions previously reported in a high-throughput automated synthetic cage screen (Table S1).[35b] Reactions were conducted in deuterated solvents to allow direct analysis prior to isolation. Species remained in solution under all conditions investigated and $^1$H NMR analysis confirmed that all reactions

had gone to completion and formed a single molecular species. In each case, high-resolution mass spectrometry (HRMS) indicated clean formation of a **Tet$^3$Di$^6$** cage species. Following this successful cage formation, the remaining 6 ditopic amines from the computational modelling were screened (Table S2), with the aim of incorporating a more flexible diamine into the cage structure, as it was thought that the highly pre-configured CHDA linker could potentially prevent the cage from having enough rotational freedom to photoisomerize. However, many of the ditopic amines screened resulted in precipitates forming over the course of the reaction, suggesting that insoluble polymer was formed – this disrupts the equilibrium of species in solution and reduces the amount of cage that can be formed in the reaction, if any cage was formed. In all of these cases, analysis by $^1$H NMR spectroscopy indicated either the reaction had not gone to completion or no soluble molecular species were present. However, HRMS indicated trace formation of a further three **Tet$^3$Di$^6$** cages, alongside a **Tet$^2$Di$^4$** cage that formed with 1,3-diaminopropane (Table S2).

Next, the ditopic diazene aldehyde was screened with the same selection of tritopic amines as computationally modelled (Table S3). The same conditions were used as for the previous screen with the tetratopic diazene aldehyde. In all combinations, **Tri$^2$Di$^3$** cages were formed as indicated by HRMS. However, only the combination with tris(2-aminoethyl)amine (TREN) formed a **Tri$^2$Di$^3$** cage in high conversion as indicated by $^1$H NMR analysis, with the other combinations containing large amounts of insoluble precipitate and residual aldehyde.

Based on these synthetic screens, two azobenzene-covalent cages (**ACC**) were discovered with high conversion: **ACC-1** formed from the tetratopic aldehyde with CHDA in a **Tet$^3$Di$^6$** topology, and **ACC-2** formed from the ditopic aldehyde with TREN as a **Tri$^2$Di$^3$** capsule (Fig. 3). Single crystal structures were grown directly from the reaction solutions by vapour diffusion with ethanol, confirming the cage topologies (SCXRD **ACC-1** Fig. S2, **ACC-2** Fig. S5). Isolation of the bulk material found that **ACC-1** retained no crystallinity, showing only amorphous character by PXRD (Fig. S3), and **ACC-2** produced a crystalline sample that resembled the simulated powder pattern from the SCXRD data (Fig. S6).

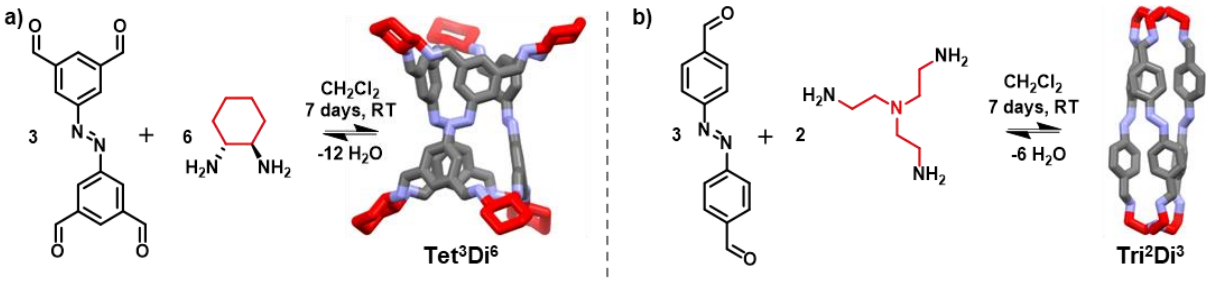


**Figure 3.** Reaction scheme for the one-pot syntheses and the corresponding crystal structures of: (a) azobenzene-covalent cage 1 (**ACC-1**) formed using 3 equivalents of 5,5'-(diazene-1,2-diyl)diisophthalaldehyde and 6 equivalents of CHDA in dichloromethane; (b) azobenzene-covalent cage 2 (**ACC-2**) formed using 3 equivalents of 4,4'-(diazene-1,2-diyl)dibenzaldehyde and 2 equivalents of TREN in dichloromethane. Hydrogens removed for clarity, aliphatic linkers shown in red, azobenzene linkers shown in grey, and nitrogens shown in blue.

We next explored the possible range of accessible photoisomers for these two cages using computational modelling. For each cage containing three diazene moieties, four species are possible: fully *trans* (*EEE*), partially isomerized (*EEZ* and *EZZ*), and fully *cis* (*ZZZ*). Models were assembled for each of these isomers for both **ACC-1** and **ACC-2**, and longer MD conformer searches performed and the relative formation energies and internal cavity diameters compared using DFT calculations at the

PBE/TZVP+D3 level (Fig. 4).[40] In both cases, the relative energy of the *ZZZ*-configuration was the highest, and the *EEE*-configuration was the lowest. The intermediate structures follow this trend, with each additional *Z*-isomer resulting in a higher relative energy. By comparison, for a triazomacrocycle reported by Heindl *et al.*,[30] the relative energy of the fully *cis*-isomer was approximately 106 kJ mol$^{-1}$ higher than the fully *trans*-isomer, and they were able to achieve 73% isomerization.

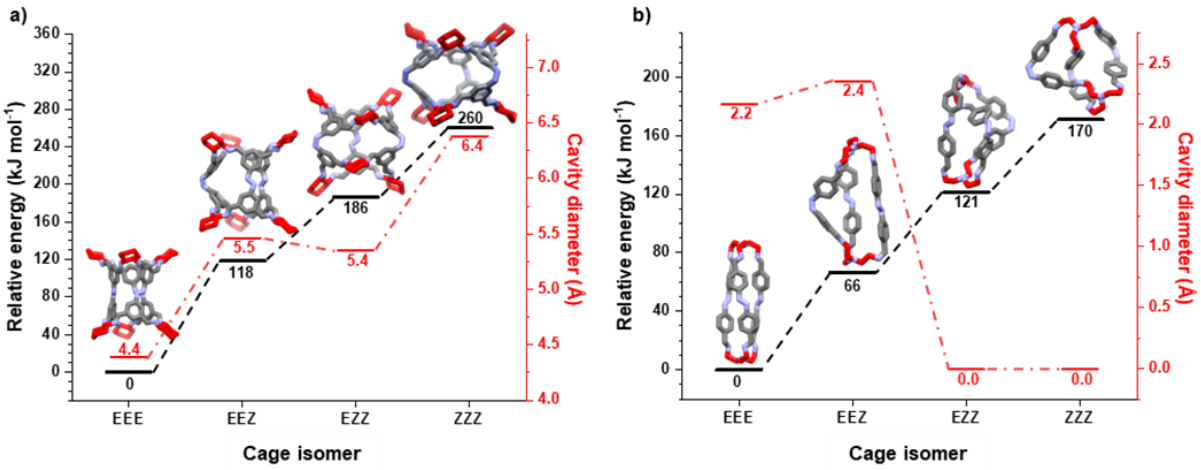


**Figure 4.** Relative energy (kJ mol$^{-1}$) for each isomeric state, *EEE*, *EEZ*, *EZZ*, *ZZZ*, in black, and the corresponding intrinsic cavity diameters (Å) from DFT simulations at the PBE/TZVP-D3 level in red: (a) azobenzene-organic cage 1 (**ACC-1**); (b) azobenzene-organic cage 2 (**ACC-2**).

The internal cavity diameters of both cages were also calculated from these computational models. **ACC-1** has a larger internal cavity than **ACC-2** in all isomeric states. When in the fully *trans*-configuration (*EEE*), **ACC-1** has an internal spherical cavity diameter of 4.4 Å, which increases to 6.4 Å when in the *ZZZ*-configuration. The change in cavity size is not simply monotonic with isomerization, and there is a small decrease in cavity size between the *EEZ*- and *EZZ*-forms (5.5 to 5.4 Å). By contrast, there is predicted to be a complete loss of the internal cavity for **ACC-2** in its *EZZ*- and *ZZZ*-configurations, although there is an initial increase in spherical cavity diameter from *EEE* to *EEZ* of 2.2 to 2.4 Å. As well as the size, as can be seen from Figure 4, the shape of the cavity also changes considerably. In principle, both the size and shape could be exploited to allow small gas molecules to be selectively adsorbed and desorbed; unfortunately, it was found that neither of the two cages could adsorb $N_2$ (77 K), $CO_2$ or $CH_4$ (273 K) as the *EEE*-isomer in the bulk amorphous phase (Fig. S7,8), which is likely due to a lack of an interconnected pore network in the amorphous state when compared to the crystal packing observed in the SCXRD for cage solvates, particularly for the **Tet$^3$Di$^6$** species (Fig. S2).

With both cages producing feasibly energetically accessible[30] calculated relative energies across the different isomer conformations, the photoisomerization behaviour was explored using UV–Vis spectroscopy (Fig. 5a-b). In each case, the cages were dissolved in dry dichloroethane (DCE) with concentrations of ca. 30 µM with respect to the azobenzene unit for both cages. Each system was irradiated with light from the initial *EEE* solution (dark state) to a *Z*-rich photostationary state (PSS). **ACC-1** was irradiated with both 340 nm and 365 nm light, achieving a conversion of 77% and 75% to *ZZZ*-**ACC-1** respectively. Conversion back to the *EEE*-rich solution was also successful using 405 nm and 450 nm light, which produced 94% of *EEE*-**ACC-1**. Irradiation of **ACC-2** with 365 nm light gave a PSS of only 54% *ZZZ*-**ACC-2**, whilst irradiation with 450 nm light produced a 97% *EEE*-**ACC-2** solution. The

previously reported reduced variant of **ACC-2** also shows higher conversion to *ZZZ* with a reported value of 87%,[31a] showing how the varied flexibility and electronic effects between imine and amine bonds plays an important role in the photoisomerization of cage molecules. **ACC-1** exhibited the longer thermal half-life of the two cages at 110 ± 10 hours in dry DCE at 25 °C as measured by UV–Vis (Fig. S9–10), compared to 6.0 ± 0.1 hours for **ACC-2** (Fig. S11).

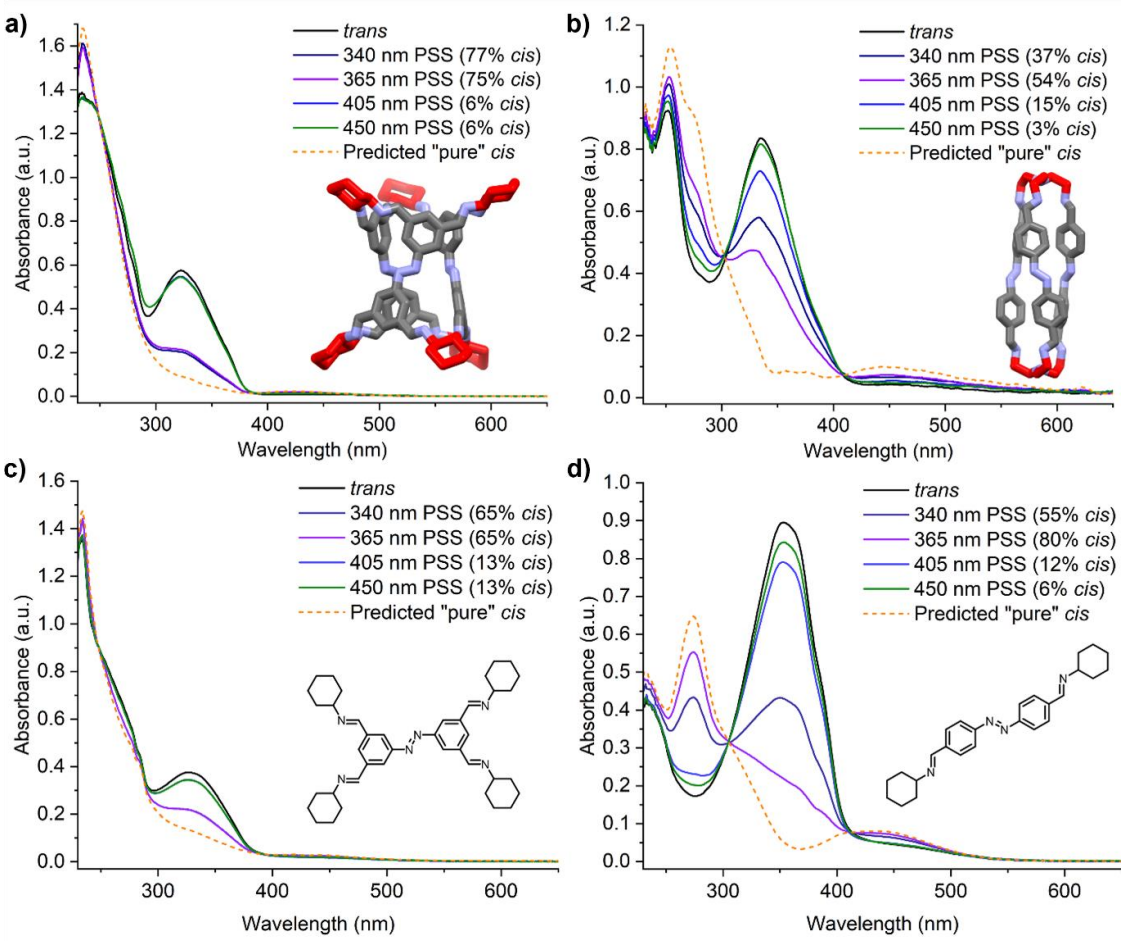


**Figure 5.** The UV–Vis spectra of azobenzene-derived cages, (a) **ACC-1** and (b) **ACC-2**, measured at 20 °C in dry DCE (ca. 30 µM with respect to the azobenzene units), and single azobenzene subunits used as a comparison to their respective cages, (c) **A1** and (d) **A2**, measured at 20 °C in dry DCE (30 µM). The percentage of the *cis*-isomer present at the PSS of each irradiation wavelengths is shown, and the "pure" fully *cis* spectrum overlaid (dashed line).

The photoisomerization properties of single azobenzene subunits with imine moieties, **A1** and **A2** (Fig. 5c-d), were also characterized to determine the influence of cage formation on both the PSS and thermal half-life in dry DCE (ca. 30 µM) (Fig. S13–16). Interestingly, the single azobenzene unit **A1** showed lower conversion for both *E*→*Z* (65% vs 77%) and *Z*→*E* (87% vs 94%) photoswitching over **ACC-1**, whilst **A2** displayed a higher conversion for *E*→*Z* (80% vs 54%) and *Z*→*E* (94% vs 97%) than **ACC-2**. This suggests that there is a structural effect in the cage which influences the switching. The impact of cage formation on the thermal half-life did not affect the photoswitches similarly. At 25 °C, **A1** displayed a half-life of 220 ± 70 hours—approximately double that of **ACC-1** (*i.e.*, cage formation resulted in a less stable *Z*-isomer), while **A2** had a half-life of 4.78 ± 0.01 hours, meaning that cage formation improved the overall *Z*-isomer stability. A summary of the photoswitching properties is provided in Table 1, alongside their overall enthalpy ($\Delta H^{\ddagger}$) and entropy ($\Delta S^{\ddagger}$) of activation obtained via

Eyring plots at elevated temperatures, though caution should be applied in the physical interpretation of the transition state parameters as the *ZZZ*→*EEE* conversion is a result of multiple sequential isomerization processes.

**Table 1.** Summary of photoswitching properties for cages and azobenzene subunits in this study.

| | Tetratopic | | Ditopic | |
|---|---|---|---|---|
| | **A1** | **ACC-1** | **A2** | **ACC-2** |
| Best *E*–*Z* PSS | 65% *cis* | 77% *cis* | 80% *cis* | 54% *cis* |
| Best *Z*–*E* PSS | 13% *cis* | 6% *cis* | 6% *cis* | 3% *cis* |
| $t_{1/2}$ (25 °C) / h | 220 ± 70 | 110 ± 10 | 4.78 ± 0.01 | 6.0 ± 0.1 |
| $\Delta H^{\ddagger}$ / kJ mol$^{-1}$ | 102 ± 7 | 104 ± 2 | 107 ± 8 | 83 ± 2 |
| $\Delta S^{\ddagger}$ / J K$^{-1}$ mol$^{-1}$ | -20 ± 20 | -7 ± 6 | 30 ± 30 | -51 ± 7 |

Due to its superior photoswitching properties, UV–Vis absorption profiles for the individual photoisomers of **ACC-1** were subsequently obtained by irradiation of a sample dissolved in dry DCE with 365 nm light and subsequent separation by HPLC. Their individual UV–Vis spectra show an expected decrease in the π–π* absorption intensity upon isomerization to *ZZZ*-**ACC-1** (Fig. S19–20). Unexpectedly, the absorption profiles of *EEE*- and *EEZ*-**ACC-1** appear almost identical after normalization to the isosbestic point, with no apparent change in the π–π* intensity.

Finally, both the forward switching of **ACC-1**, and its thermal relaxation, after irradiation with 340 nm light was followed via $^{1}$H NMR spectroscopy in either $d_4$-DCE at ambient temperature (Fig. S21-22) or dry DCE with solvent suppression at 35 °C (Fig. 6, S25–28), respectively. The former study was used to identify each of the individual *EEE*, *EEZ*, *EZZ*, and *ZZZ* isomers of the cage. Half-lives of the intermediate photoisomers were calculated by fitting data to a stepwise series of first-order reactions, resulting in individual half-lives of: 3.74 ± 0.02 hours (*ZZZ*→*EZZ*); 11.83 ± 0.08 hours (*EZZ*→*EEZ*); and 3.4 ± 0.1 hours (*EEZ*→*EEE*). The thermally induced isomerization of *EZZ* to *EEZ* has the longest half-life, which correlates with the comparatively smaller difference in relative energy of the photoisomers (Fig. 4a). Compared to the azobenzene subunit **A1**, all photoisomers have a reduced thermal half-life due to increased cage strain energy with each additional *Z*-isomer.

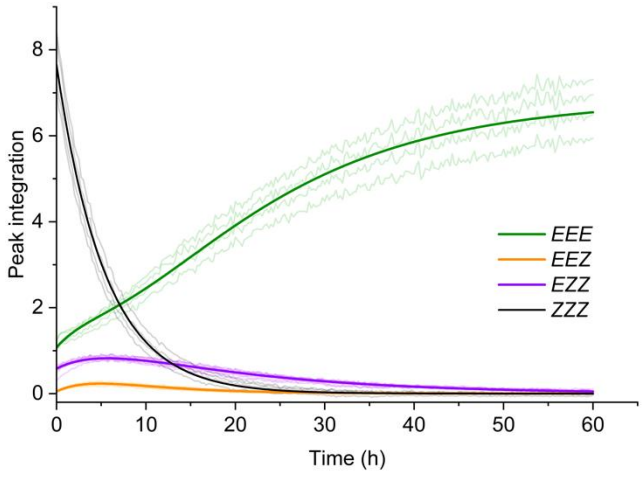


**Figure 6.** Kinetics of **ACC-1** thermal isomerization followed by $^{1}$H NMR spectroscopy (35 °C, dry DCE). The peak integrations (faded lines) were fit to sequential first order rates (solid lines).

## Conclusions

In conclusion, two photoresponsive organic cages, **ACC-1** and **ACC-2**, incorporating azobenzene functionality have been realised and their photoisomerization properties studied. Computational modelling led to the discovery of plausible photoswitchable cages using synthetically accessible precursors. By screening a range of diamines and triamines, two promising cage candidates were identified, isolated, and characterized. After successfully synthesizing these cages, a series of UV–Vis experiments were utilised to explore their photophysical properties. Both cages were found to be capable of photoisomerization, where **ACC-1** (**Tet$^{3}$Di$^{2}$** cage) was found to have a PSS of 77% of the *cis*-isomer with 340 nm light and had a thermal half-life of 110 ± 10 hours. The second smaller cage, **ACC-2** (**Tri$^{2}$Di$^{3}$** cage) had a PSS of 54% (365 nm) of the *cis*-isomer and a thermal half-life of 6.0 ± 0.1 hours. The individual isomers of **ACC-1** were subsequently separated by HPLC, and their individual UV–Vis spectra obtained accordingly. Analysis of the photoisomers of **ACC-1** by $^{1}$H NMR spectroscopy enabled determination of their thermal half-lives, indicating a comparatively stable *EZZ*-isomer. The photoisomerizability of these cages was also supported by relative energy calculations, further demonstrating that computational design can be used to tackle this problem. These photoswitching experiments were carried out in solution; future work will focus on discovering functional porous organic cage materials that can be switched in the solid state.

**References**

(1) Dusselier, M.; Davis, M. E. Small-Pore Zeolites: Synthesis and Catalysis. Chem. Rev. 2018, 118 (11), 5265-5329.

(2) Morris, R. E.; Wheatley, P. S. Gas Storage in Nanoporous Materials. Angew. Chem. Int. Ed. 2008, 47 (27), 4966-4981.

(3) Li, X.; Liu, Y.; Wang, J.; Gascon, J.; Li, J.; Van der Bruggen, B. Metal–organic frameworks based membranes for liquid separation. Chem. Soc. Rev. 2017, 46 (23), 7124-7144.

(4) (a) Furukawa, H.; Cordova, K. E.; O'Keeffe, M.; Yaghi, O. M. The Chemistry and Applications of Metal-Organic Frameworks. Science. 2013, 341 (6149), 1230444. (b) Ding, S.-Y.; Wang, W. Covalent organic frameworks (COFs): from design to applications. Chem. Soc. Rev. 2013, 42 (2), 548-568. (c) Briggs, M. E.; Cooper, A. I. A Perspective on the Synthesis, Purification, and Characterization of Porous Organic Cages. Chem. Mater. 2017, 29 (1), 149-157. (d) Rowan, S. J.; Cantrill, S. J.; Cousins, G. R. L.; Sanders, J. K. M.; Stoddart, J. F. Dynamic Covalent Chemistry. Angew. Chem. Int. Ed. 2002, 41 (6), 898-952.

(5) Tozawa, T.; Jones, J. T. A.; Swamy, S. I.; Jiang, S.; Adams, D. J.; Shakespeare, S.; Clowes, R.; Bradshaw, D.; Hasell, T.; Chong, S. Y.; et al. Porous organic cages. Nat. Mater. 2009, 8 (12), 973-978.

(6) (a) Yang, X.; Ullah, Z.; Stoddart, J. F.; Yavuz, C. T. Porous Organic Cages. Chem. Rev. 2023, 123 (8), 4602-4634. (b) Hu, D.; Zhang, J.; Liu, M. Recent advances in the applications of porous organic cages. Chem. Commun. 2022, 58 (81), 11333-11346.

(7) Wang, W.; Su, K.; Yuan, D. Porous organic cages for gas separations. Mater. Chem. Front. 2023, 7 (21), 5247-5262.

(8) Liu, M.; Zhang, L.; Little, M. A.; Kapil, V.; Ceriotti, M.; Yang, S.; Ding, L.; Holden, D. L.; Balderas-Xicohténcatl, R.; He, D.; et al. Barely porous organic cages for hydrogen isotope separation. Science. 2019, 366 (6465), 613-620.

(9) (a) Yuan, S.; Zou, L.; Qin, J.-S.; Li, J.; Huang, L.; Feng, L.; Wang, X.; Bosch, M.; Alsalme, A.; Cagin, T.; et al. Construction of hierarchically porous metal–organic frameworks through linker labilization. Nat. Commun. 2017, 8 (1), 15356. (b) Chen, L.; Reiss, P. S.; Chong, S. Y.; Holden, D.; Jelfs, K. E.; Hasell, T.; Little, M. A.; Kewley, A.; Briggs, M. E.; Stephenson, A.; et al. Separation of rare gases and chiral molecules by selective binding in porous organic cages. Nat. Mater. 2014, 13 (10), 954-960.

(10) Lu, Z.; Lu, X.; Zhong, Y.; Hu, Y.; Li, G.; Zhang, R. Carbon dot-decorated porous organic cage as fluorescent sensor for rapid discrimination of nitrophenol isomers and chiral alcohols. Anal. Chim. Acta. 2019, 1050, 146-153.

(11) (a) Giri, N.; Del Pópolo, M. G.; Melaugh, G.; Greenaway, R. L.; Rätzke, K.; Koschine, T.; Pison, L.; Gomes, M. F. C.; Cooper, A. I.; James, S. L. Liquids with permanent porosity. Nature. 2015, 527 (7577), 216-220. (b) O'Reilly, N.; Giri, N.; James, S. L. Porous Liquids. Chem. Eur. J. 2007, 13 (11), 3020-3025.

(12) (a) Cai, W.; Wang, J.; Chu, C.; Chen, W.; Wu, C.; Liu, G. Metal–Organic Framework-Based Stimuli-Responsive Systems for Drug Delivery. Adv. Sci. 2019, 6 (1), 1801526. (b) Haldar, R.; Heinke, L.; Wöll, C. Advanced Photoresponsive Materials Using the Metal–Organic Framework Approach. Adv. Mater.

2020, 32 (20), 1905227. (c) Jones, C. L.; Tansell, A. J.; Easun, T. L. The lighter side of MOFs: structurally photoresponsive metal–organic frameworks. J. Mater. Chem. 2016, 4 (18), 6714-6723.

(13) (a) Hartley, G. S. The Cis-form of Azobenzene. Nature. 1937, 140 (3537), 281. (b) Tamai, N.; Miyasaka, H. Ultrafast Dynamics of Photochromic Systems. Chem. Rev. 2000, 100 (5), 1875-1890.

(14) Turanský, R.; Konôpka, M.; Doltsinis, N. L.; Štich, I.; Marx, D. Switching of functionalized azobenzene suspended between gold tips by mechanochemical, photochemical, and opto-mechanical means. Phys. Chem. Chem. Phys. 2010, 12 (42), 13922-13932.

(15) Liu, Z. F.; Hashimoto, K.; Fujishima, A. Photoelectrochemical information storage using an azobenzene derivative. Nature. 1990, 347 (6294), 658-660.

(16) (a) Das, G.; Prakasam, T.; Addicoat, M. A.; Sharma, S. K.; Ravaux, F.; Mathew, R.; Baias, M.; Jagannathan, R.; Olson, M. A.; Trabolsi, A. Azobenzene-Equipped Covalent Organic Framework: Light-Operated Reservoir. J. Am. Chem. Soc. 2019, 141 (48), 19078-19087. (b) Prasetya, N.; Ladewig, B. P. Dynamic photo-switching in light-responsive JUC-62 for CO2 capture. Sci. Rep. 2017, 7 (1), 13355. (c) Lyndon, R.; Konstas, K.; Ladewig, B. P.; Southon, P. D.; Kepert, C. J.; Hill, M. R. Dynamic Photo-Switching in Metal–Organic Frameworks as a Route to Low-Energy Carbon Dioxide Capture and Release. Angew. Chem. Int. Ed. 2013, 52 (13), 3695-3698.

(17) (a) Meng, X.; Gui, B.; Yuan, D.; Zeller, M.; Wang, C. Mechanized azobenzene-functionalized zirconium metal-organic framework for on-command cargo release. Sci. Adv. 2016, 2 (8), e1600480. (b) Huang, R.; Hill, M. R.; Babarao, R.; Medhekar, N. V. CO2 Adsorption in Azobenzene Functionalized Stimuli Responsive Metal–Organic Frameworks. J. Phys. Chem. C. 2016, 120 (30), 16658-16667.

(18) Waldeck, D. H. Photoisomerization dynamics of stilbenes. Chem. Rev. 1991, 91 (3), 415-436.

(19) (a) Bandara, H. M. D.; Burdette, S. C. Photoisomerization in different classes of azobenzene. Chem. Soc. Rev. 2012, 41 (5), 1809-1825. (b) Ciminelli, C.; Granucci, G.; Persico, M. The Photoisomerization Mechanism of Azobenzene: A Semiclassical Simulation of Nonadiabatic Dynamics. Chem. Eur. J. 2004, 10 (9), 2327-2341.

(20) Tian, H.; Yang, S. Recent progresses on diarylethene based photochromic switches. Chem. Soc. Rev. 2004, 33 (2), 85-97.

(21) Klajn, R. Spiropyran-based dynamic materials. Chem. Soc. Rev. 2014, 43 (1), 148-184.

(22) Wu, J.; Kreimendahl, L.; Tao, S.; Anhalt, O.; Greenfield, J. L. Photoswitchable imines: aryliminopyrazoles quantitatively convert to long-lived Z-isomers with visible light. Chem. Sci. 2024, 15 (11), 3872-3878.

(23) Rodier, J. M.; Myers, A. B. cis-Stilbene photochemistry: solvent dependence of the initial dynamics and quantum yields. J. Am. Chem. Soc. 1993, 115 (23), 10791-10795.

(24) Malkin, Y. N.; Krasieva, T. B.; Kuzmin, V. A. Quantitative study of the photostability of spiropyrans. J. Photochem. Photobiol., A. 1989, 49 (1), 75-88.

(25) Brand, M. C.; Trowell, H. G.; Fuchter, M. J.; Greenaway, R. L. Incorporating Photoresponses into Porous Liquids. Chem. Eur. J. 2024, 30 (16), e202303593.

(26) (a) Hermann, D.; Emerich, H.; Lepski, R.; Schaniel, D.; Ruschewitz, U. Metal–Organic Frameworks as Hosts for Photochromic Guest Molecules. Inorg. Chem. 2013, 52 (5), 2744-2749. (b) Knebel, A.; Sundermann, L.; Mohmeyer, A.; Strauß, I.; Friebe, S.; Behrens, P.; Caro, J. Azobenzene Guest Molecules as Light-Switchable CO2 Valves in an Ultrathin UiO-67 Membrane. Chem. Mater. 2017, 29 (7), 3111-3117. (c) Yanai, N.; Uemura, T.; Inoue, M.; Matsuda, R.; Fukushima, T.; Tsujimoto, M.; Isoda, S.; Kitagawa, S. Guest-to-Host Transmission of Structural Changes for Stimuli-Responsive Adsorption Property. J. Am. Chem. Soc. 2012, 134 (10), 4501-4504.

(27) (a) Heinke, L.; Cakici, M.; Dommaschk, M.; Grosjean, S.; Herges, R.; Bräse, S.; Wöll, C. Photoswitching in Two-Component Surface-Mounted Metal–Organic Frameworks: Optically Triggered Release from a Molecular Container. ACS Nano. 2014, 8 (2), 1463-1467. (b) Rice, A. M.; Martin, C. R.; Galitskiy, V. A.; Berseneva, A. A.; Leith, G. A.; Shustova, N. B. Photophysics Modulation in Photoswitchable Metal–Organic Frameworks. Chem. Rev. 2020, 120 (16), 8790-8813. (c) Brown, J. W.; Henderson, B. L.; Kiesz, M. D.; Whalley, A. C.; Morris, W.; Grunder, S.; Deng, H.; Furukawa, H.; Zink, J. I.; Stoddart, J. F.; et al. Photophysical pore control in an azobenzene-containing metal–organic framework. Chem. Sci. 2013, 4 (7), 2858-2864.

(28) (a) Song, W.-C.; Cui, X.-Z.; Liu, Z.-Y.; Yang, E.-C.; Zhao, X.-J. Light-triggered Supramolecular Isomerism in a Self-catenated Zn(II)-organic Framework: Dynamic Photo-switching CO2 Uptake and Detection of Nitroaromatics. Sci. Rep. 2016, 6 (1), 34870. (b) Baroncini, M.; d'Agostino, S.; Bergamini, G.; Ceroni, P.; Comotti, A.; Sozzani, P.; Bassanetti, I.; Grepioni, F.; Hernandez, T. M.; Silvi, S.; et al. Photoinduced reversible switching of porosity in molecular crystals based on star-shaped azobenzene tetramers. Nat. Chem. 2015, 7 (8), 634-640.

(29) Oldknow, S.; Martir, D. R.; Pritchard, V. E.; Blitz, M. A.; Fishwick, Colin W. G.; Zysman-Colman, E.; Hardie, M. J. Structure-switching M3L2 Ir(III) coordination cages with photo-isomerising azo-aromatic linkers. Chem. Sci. 2018, 9 (42), 8150-8159.

(30) Heindl, A. H.; Becker, J.; Wegner, H. A. Selective switching of multiple azobenzenes. Chem. Sci. 2019, 10 (31), 7418-7425.

(31) (a) Yuan, T.; Wang, Z.-Q.; Gong, X.-Q.; Wang, Q. Cage structure helps to improve the photoisomerization efficiency of azobenzene. Tetrahedron Lett. 2020, 61 (50), 152626. (b) Chen, D.; Guo, Q.; Wang, J.; Wang, K.; Wang, Q. Regulating the photoisomerization pathway to achieve efficient E→Z isomerization of azobenzene-embedded molecular cages. Tetrahedron Lett. 2024, 143, 155110.

(32) Ovalle, M.; Kathan, M.; Toyoda, R.; Stindt, C. N.; Crespi, S.; Feringa, B. L. Light-Fueled Transformations of a Dynamic Cage-Based Molecular System. Angew. Chem. Int. Ed. 2023, 62 (9), e202214495.

(33) Moosa, B.; Alimi, L. O.; Shkurenko, A.; Fakim, A.; Bhatt, P. M.; Zhang, G.; Eddaoudi, M.; Khashab, N. M. A Polymorphic Azobenzene Cage for Energy-Efficient and Highly Selective p-Xylene Separation. Angew. Chem. Int. Ed. 2020, 59 (48), 21367-21371.

(34) Oshchepkov, A. S.; Namashivaya, S. S. R.; Khrustalev, V. N.; Hampel, F.; Laikov, D. N.; Kataev, E. A. Control of Photoisomerization of an Azoazacryptand by Anion Binding and Cucurbit[8]uril Encapsulation in an Aqueous Solution. J. Org. Chem. 2020, 85 (14), 9255-9263.

(35) (a) Slater, A. G.; Little, M. A.; Pulido, A.; Chong, S. Y.; Holden, D.; Chen, L.; Morgan, C.; Wu, X.; Cheng, G.; Clowes, R.; et al. Reticular synthesis of porous molecular 1D nanotubes and 3D networks. Nat. Chem. 2017, 9 (1), 17-25. (b) Greenaway, R. L.; Santolini, V.; Bennison, M. J.; Alston, B. M.; Pugh, C. J.; Little, M. A.; Miklitz, M.; Eden-Rump, E. G. B.; Clowes, R.; Shakil, A.; et al. High-throughput discovery of organic cages and catenanes using computational screening fused with robotic synthesis. Nat. Commun. 2018, 9 (1), 2849. (c) Acharyya, K.; Mukherjee, S.; Mukherjee, P. S. Molecular Marriage through Partner Preferences in Covalent Cage Formation and Cage-to-Cage Transformation. J. Am. Chem. Soc. 2013, 135 (2), 554-557. (d) Lauer, J. C.; Zhang, W.-S.; Rominger, F.; Schröder, R. R.; Mastalerz, M. Shape-Persistent [4+4] Imine Cages with a Truncated Tetrahedral Geometry. Chem. Eur. J. 2018, 24 (8), 1816-1820.

(36) Santolini, V.; Miklitz, M.; Berardo, E.; Jelfs, K. E. Topological landscapes of porous organic cages. Nanoscale. 2017, 9 (16), 5280-5298.

(37) Turcani, L.; Berardo, E.; Jelfs, K. E. stk: A python toolkit for supramolecular assembly. J. Comput. Chem. 2018, 39 (23), 1931-1942.

(38) Roos, K.; Wu, C.; Damm, W.; Reboul, M.; Stevenson, J. M.; Lu, C.; Dahlgren, M. K.; Mondal, S.; Chen, W.; Wang, L.; et al. OPLS3e: Extending Force Field Coverage for Drug-Like Small Molecules. J. Chem. Theory Comput. 2019, 15 (3), 1863-1874.

(39) Miklitz, M.; Jelfs, K. E. pywindow: Automated Structural Analysis of Molecular Pores. J. Chem. Inf. Model. 2018, 58 (12), 2387-2391.

(40) (a) Perdew, J. P.; Burke, K.; Ernzerhof, M. Generalized Gradient Approximation Made Simple. Phys. Rev. Lett. 1996, 77 (18), 3865-3868. (b) Grimme, S.; Antony, J.; Ehrlich, S.; Krieg, H. A consistent and accurate ab initio parametrization of density functional dispersion correction (DFT-D) for the 94 elements H-Pu. J. Chem. Phys. 2010, 132 (15), 154104.

## Author Contributions

M.C.B., J.T.P., K.E.J. and R.L.G. conceived the project. M.C.B. synthesised, isolated and characterised the precursors and cages, carried out the crystallisation screens and sorption measurements. M.A.L. collected and interpreted the SCXRD data. M.C.B., H.G.T., J.L.G., and M.O. carried out the UV-Vis studies, M.C.B. and H.G.T. carried out the switching and thermal relaxation studies by $^{1}$H NMR spectroscopy with assistance from P.R.H., and H.G.T. conducted the thermal half-life calculations. N.R. provided technical assistance and 3D printed components for sample irradiation. J.T.P. carried out the computational modelling, led by K.E.J. The paper was written, reviewed and edited by M.C.B., H.G.T., K.E.J. and R.L.G. with input from all authors, M.J.F., AI.C., K.E.J. and R.L.G. acquired the funding and provided supervision, with R.L.G. directing the overall project.


## Funding Sources

This work was financially supported by the Engineering and Physical Sciences Research Council (EPSRC, EP/R005710/1, EP/R00188X/1), and the Leverhulme Trust (RPG-2018-051 and the Leverhulme Research Centre for Functional Materials Design). K.E.J. and R.L.G. thank the Royal Society for University Research Fellowships. K. E. J. acknowledges the ERC through Agreement No. 758370 (ERC-StG-PE5- CoMMaD). H.G.T thanks the EPSRC CDT React for financial support under EP/S023232/1. M.O. thanks Imperial College for a President's PhD Scholarship. This project was supported by access to instrumentation at the Centre for Rapid Online Analysis of Reactions (ROAR) at Imperial College London (EPSRC, EP/R008825/1 and EP/V029037/1). This work used the ARCHER2 UK National Supercomputing Service (https://www.archer2.ac.uk) via our membership of the UK's HEC Materials Chemistry Consortium, which is funded by EPSRC (EP/R029431), and Imperial College London's Research Computing Service, DOI: 10.14469/hpc/2232.

## Acknowledgements

We thank Andrew Marsh for the synthesis of (2,4,6-trimethylbenzene-1,3,5-triyl)trimethanamine, Stephen Moss, Scott Christy, David Vega Herrera, and the MicroBioRefinery for assistance with QTOF-MS measurements, and Chris Roberts for assistance with the HPLC method development in ROAR.



## Corresponding Author

Correspondence to R. L. Greenaway


## Competing Interests

The authors declare no competing interests.